Nano Energy (2015) 17, 17–26

Available online at www.sciencedirect.com

ScienceDirect

journal homepage: www.elsevier.com/locate/nanoenergy

RAPID COMMUNICATION

Novel cobalt oxide-nanobubble-decorated reduced graphene oxide sphere with superior electrochemical properties prepared by nanoscale Kirkendall diffusion process

Gi Dae Park, Jung Sang Cho, Yun Chan Kang*

Department of Materials Science and Engineering, Korea University, Anam-Dong, Seongbuk-Gu, Seoul 136-713, Republic of Korea

Received 11 March 2015; received in revised form 29 May 2015; accepted 28 July 2015
Available online 5 August 2015

KEYWORDS
Kirkendall diffusion;
Graphene composite;
Lithium ion battery;
Spray pyrolysis

Abstract
In this study, a novel metal oxide–reduced graphene oxide (RGO) composite structure, denoted as a "nanobubble-decorated RGO sphere," was fabricated and characterized for potential use in Li^+-ion batteries. The nanobubble-decorated RGO sphere consists of an RGO sphere uniformly decorated with hollow metal oxide nanopowder. Reduction of the composite powder prepared by spray pyrolysis under H_2/Ar gas mixture formed RGO spheres decorated with metal nanopowders. The metal nanopowders were transformed into hollow metal oxide nanopowders, or nanobubbles, by the nanoscale Kirkendall diffusion process. Cobalt oxide nanobubble-decorated RGO spheres, prepared as the first target material, showed excellent Li-storage properties. The cobalt oxide–RGO composite powders, tested at the current density of 2 A g^{-1} for 200 cycles before and after the nanoscale Kirkendall diffusion, showed discharge capacities of 932 and 1156 mA h g^{-1}, respectively; their capacity retentions measured from the second cycle onward were 89% and 99%, respectively.

Introduction

Energy storage devices such as rechargeable Li-ion batteries (LIBs) have recently become one of the more important energy sources [1–9]. To achieve rechargeable LIBs with superior electrochemical properties, nanostructured transition metal oxide materials that exhibit high specific capacities, fast rate-performances, and long cycle lives have been developed [10–16]. Nano-sized hollow metal oxide powders used as energy storage materials exhibit good electrochemical properties at

*Corresponding author. Tel.: +82 2 928 3268; fax: +82 2 3290 3584.
E-mail address: yckang@korea.ac.kr (Y.C. Kang).

http://dx.doi.org/10.1016/j.nanoen.2015.07.026
2211-2855/

high current densities because of their shortened diffusion length and increased contact area with the electrolyte for Li^+ insertion/extraction [17-25]. In addition, the hollow structure can accommodate the large volume change that occurs during the repeated Li insertion and desertion processes. The use of organic and inorganic templates is a popular method to fabricate nano-sized hollow metal oxide powders [22-27]. The elimination of the template, usually by chemical etching, produced nano-sized hollow powders for use in LIB anode materials. Nano-sized hollow powders have been also successfully prepared without the use of templates by nanoscale Kirkendall diffusion using metal nanopowders [28-35]. The difference in the rates of outward diffusion of metal cations through the oxide layer and inward diffusion of oxygen into the metals during the oxidation process resulted in a hollow metal oxide nanopowder [32-35]. These hollow nanopowders have usually been prepared on the lab scale within a beaker. The large-scale fabrication of hollow nanopowder by applying nanoscale Kirkendall diffusion via annealing metal powders under a non-aqueous atmosphere, e.g. in a box furnace, has scarcely been studied. As anode materials for LIBs, hollow nanopowders of several tens of nanometers in size have disadvantages regarding ease of handling and large-scale production.

Graphene is an impressive support material for electrochemically active nanomaterials because of its high electric and thermal conductivity, flexibility, large surface area, and chemical stability [36-39]. Graphene-based metal oxide composites prepared by both liquid solution and spray pyrolysis processes have shown superior electrochemical properties compared to bare metal oxides [40-45]. Reduced graphene oxide (RGO) deposited with hollow metal oxide nanopowders, mainly prepared by liquid solution processes, has also been studied as a class of anode materials for LIBs [46-49]. However, the RGO-metal oxide materials prepared by liquid solution methods have non-spherical bulk morphologies. Spherical RGO-metal oxide powder composites with well-defined sizes could be easily applied as anode materials in LIBs.

In this study, we propose a novel metal oxide-RGO composite structure, denoted as a "nanobubble-decorated RGO sphere" structure, which consists of an RGO sphere uniformly decorated with hollow metal oxide nanopowder. Co_3O_4-RGO composite powder with the nanobubble-decorated RGO sphere structure was prepared by spray pyrolysis as the first target material. The reduction process of the composite powder under a mixture of H_2 and Ar gas formed RGO spheres decorated with Co metal nanopowder. Co nanopowder was transformed into Co_3O_4 hollow nanopowder by nanoscale Kirkendall diffusion. Consequently, a two-step post-treatment process formed the Co_3O_4-nanobubble-decorated RGO spheres. The Co_3O_4 hollow nanopowder was found to have an ideal structure and showed superior electrochemical properties as anode material for LIBs compared to filled-structure nanopowder of the similar size.

Experimental section

Synthesis of Co_3O_4-nanobubble-decorated RGO spheres

A three-step process prepared the Co_3O_4-nanobubble-decorated RGO spheres. CoO_x-RGO spheres were prepared by spray pyrolysis using a spray solution of cobalt nitrate hexahydrate ($Co(NO_3)_2 \cdot 6H_2O$) and graphene oxide (GO). GO was synthesized from graphite flakes using a modified Hummers method, as described in our previous report [43-45]. As-synthesized GO was re-dispersed in distilled water and then exfoliated by ultrasonication to obtain GO sheets. 0.03 M of $Co(NO_3)_2 \cdot 6H_2O$ (Junsei Chemical Co., Ltd.) was dissolved in 500 mL of 1 mg mL^{-1} exfoliated GO dispersion to fabricate the CoO_x-RGO sphere precursor. In the spray pyrolysis process, droplets were generated using a 1.7-MHz ultrasonic spray generator consisting of six vibrators. The droplets were carried to a quartz reactor of length 1200 mm and diameter 50 mm, using N_2 as the carrier gas at a flow rate of 10 L min^{-1}. The reactor temperature was maintained at 500 °C. The first-step post-treatment process at 400 °C for 3 h under a 10% H_2/Ar reducing atmosphere produced a spherical Co-RGO powder. The second-step post-treatment process of the Co-RGO sphere powder at 300 °C for 3 h in air produced Co_3O_4-nanobubble-decorated RGO spheres.

Characterization

The crystal structures of the powders were investigated using X-ray diffractometry (XRD, X'pert PRO MPD) with Cu-Kα radiation (λ=1.5418 Å) at the Korea Basic Science Institute (Daegu). The morphologies of the powders were investigated using field-emission scanning electron microscopy (FE-SEM, Hitachi S-4800) and high-resolution transmission electron microscopy (HR-TEM, JEOL JEM-2100F) at a working voltage of 200 kV. The specific surface areas of the powders before and after post-treatment at various temperatures were calculated by a Brunauer-Emmett-Teller (BET) analysis of nitrogen-adsorption measurements (TriStar 3000). The X-ray photoelectron spectroscopy of the powders was performed using ESCALAB-250 with Al Kα radiation (1486.6 eV). To determine the amount of reduced graphene oxide in the cobalt oxide-RGO sphere powder, thermogravimetric analysis (TGA, SDT Q600) was performed in air at a heating rate of 10 °C min^{-1}.

Electrochemical measurements

The electrochemical properties of the powder were analyzed by constructing a 2032-type coin cell. The anode was prepared by mixing the active material, carbon black, and sodium carboxymethyl cellulose (CMC) in a weight ratio of 7:2:1. Li metal and microporous polypropylene film were used as the counter electrode and the separator, respectively. The electrolyte was 1 M $LiPF_6$ in a 1:1 volume mixture of fluoroethylene carbonate-dimethyl carbonate (FEC-DMC). The discharge/charge characteristics of the samples were investigated by cycling in the 0.001-3 V potential range at various current densities. Cyclic voltammograms were measured at a scan rate of 0.07 mV s^{-1}. The dimensions of the negative electrode were 1 cm $\times$ 1 cm and the mass loading was approximately 1.2 mg cm^{-2}. Electrochemical impedance spectroscopy (EIS) of the electrode was measured over a frequency range of 0.01 Hz to 100 kHz. The cathode ($LiMn_2O_4$ yolk-shell) was prepared by mixing the active material, carbon black, and sodium carboxymethyl cellulose

(CMC) in a weight ratio of 8:1:1. For full cell assembly, the $LiMn_2O_4$ yolk-shell electrode with a loading mass of 4 mg cm^{-2} was used as a cathode, whereas the anode mass loading was kept at 0.4 mg cm^{-2}. For the full cell, the electrolyte was 1 M $LiPF_6$ dissolved in a mixture of ethylene carbonate/diethyl carbonate (EC/DEC; 1:1 v/v). The electrochemical properties of the 2032-type coin full cells were examined at 1 A g^{-1} in voltage windows between 1.5 and 4.0 V. The electrode capacity was calculated according to the weight of the anode materials.

Results and discussion

Scheme 1 depicts the preparation of Co_3O_4-nanobubble-decorated RGO spheres. The CoO_x-RGO composite powders were prepared by spray pyrolysis from a colloidal spray solution of GO nanosheets and Co precursor. One composite powder was formed from one droplet by the decomposition of cobalt nitrate into CoO_x and the thermal reduction of GO into RGO inside the tubular reactor maintained at 500 °C. Ultrafine CoO_x nanocrystals, several nanometers in size, were uniformly distributed over the spherical RGO structures. The first-step post-treatment process under a mixture of H_2 and Ar gas produced Co-RGO composite powders. The crystal growth of the metallic Co formed by the reduction of cobalt oxide resulted in Co nanopowder particles measuring several tens of nanometers. The RGO sphere minimized the crystal growth of Co metal during the long time required for the complete reduction of CoO_x into Co metal during the reduction process. The second-step post-treatment process under air oxidized the Co metal nanopowder into hollow Co_3O_4 nanopowder by the well-known nanoscale Kirkendall diffusion process. The surface oxidation of metallic Co formed a Co/Co_3O_4 core-shell structure. Co^{3+} cations diffused outward more quickly than the inward diffusion

Scheme 1 Formation mechanism of the nanobubble (Co_3O_4)-decorated RGO sphere by nanoscale Kirkendall diffusion process.

of oxygen, consistent with the larger ionic radius of O^{2-} anions (140 pm) compared to Co^{3+} cations (75 pm). Accordingly, Kirkendall voids were generated near the Co/Co_3O_4 interface during the vacancy-assisted exchange of materials via bulk interdiffusion. The complete conversion of Co metal into Co_3O_4 by nanoscale Kirkendall diffusion resulted in the formation of hollow Co_3O_4 nanopowder. The spherical and hollow structure of the CoO_x-RGO composite powder remained constant during the two-step post-treatment process. Consequently, the proposed Co_3O_4-nanobubble-decorated RGO spheres were prepared by the described three-step process, including spray pyrolysis and two steps of post-treatment processing.

The formation mechanism of the Co_3O_4-nanobubble-decorated RGO sphere was investigated based on morphological changes during the two-step post-treatment processes. The morphologies of the CoO_x- and Co metal-decorated RGO spheres are shown in Figures S1 and 1. The CoO_x-decorated RGO spheres prepared directly by spray pyrolysis had spherical, hollow structures, without aggregation of the individual particles. Ultrafine CoO_x nanocrystals below 10-nm size were uniformly distributed over the RGO layers, as shown in Figure S1d. Clear lattice fringes separated by 0.22 and 0.45 nm, which correspond to the (200) and (111) planes of CoO and Co_3O_4, respectively, were observed in the HR-TEM images shown in Figure S1d. The spherical morphology of the CoO/Co_3O_4-RGO composite powder did not change during the reduction process that formed the Co metal-decorated RGO spheres, as shown in Figure 1a and b. However, the segregation of the reduced Co formed uniformly distributed Co nanoparticles over the RGO spheres during the post-treatment at 400 °C for 3 h under an atmosphere of 10% H_2 in Ar gas. The HR-TEM images shown in Figure 1d reveal the presence of Co nanoparticles with sizes in the range of several tens of nanometers. Clear lattice fringes separated by 0.21 nm, corresponding to the (220) plane of metallic Co, were observed in the HR-TEM images shown in Figure 1d. The elemental mapping images shown in Figures S1e and 1e reveal the hollow structure and uniform distribution of Co and C components throughout over the hollow composite spheres.

The morphological changes of the Co_3O_4-nanobubble-decorated RGO spheres after post-treatment at 300 °C for 3 h in air are shown in Figure 2. The spherical morphology of the Co_3O_4-RGO composite powder remained constant during the second-step post-treatment heating process. However, the morphology of the Co_3O_4 particles decorating the RGO changed during the second-step post-treatment process. The HR-TEM images shown in Figure 2c and d reveal hollow nanopowder particles with sizes of several tens of nanometers uniformly distributed over the RGO spheres. Clear lattice fringes separated by 0.45 nm, corresponding to the (111) plane of cubic Co_3O_4, were observed in the HR-TEM images shown in Figure 2d. The selected-area electron diffraction (SAED) pattern shown as an inset image in Figure 2d reveals the formation of cubic-phase Co_3O_4 nanospheres by nanoscale Kirkendall diffusion. HR-TEM images also confirm the ultrafine Co_3O_4 crystals, several nanometers in size, comprising each hollow nanosphere. The elemental mapping images shown in Figure 2e reveal the existence of RGO in the Co_3O_4-nanobubble-decorated RGO sphere even after the oxidation process at 300 °C.

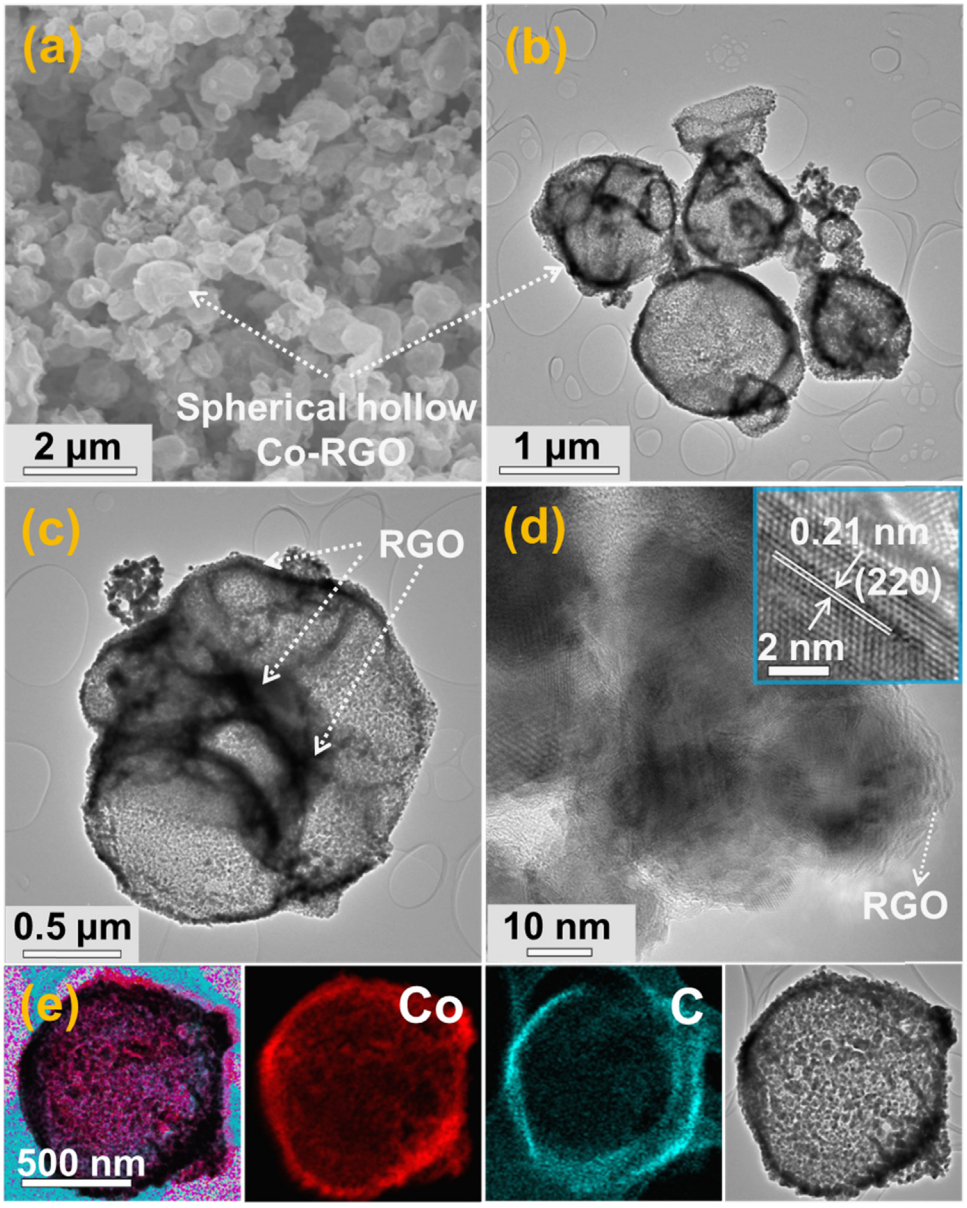

Figure 1 Morphologies and elemental mapping images of the Co metal-decorated RGO spheres post-treated at 400 °C under an atmosphere of 10% H_2 in Ar gas. (a) SEM image; (b,c) TEM images; (d) HR-TEM image; and (e) elemental mapping images.

To prepare hollow metal oxide nanopowder by nanoscale Kirkendall diffusion, a metallic nanopowder must be successfully formed. Therefore, the crystal structures and compositions of the powders obtained by each step were evaluated by XRD and XPS analysis, respectively. The XRD patterns of the three samples at different stages of the fabrication process are shown in Figure 3a. The composite powders prepared directly by spray pyrolysis show a poor-quality crystal structure of mixed Co_3O_4 and CoO phases, due to the low preparation temperature of 500 °C under N_2. The XRD pattern of the composite powder after reduction at 400 °C shows main peaks corresponding to metallic Co and smaller peaks indicating the CoO phase, showing that the ultrafine Co nanocrystals were partially oxidized under atmospheric conditions. The broad peaks of the metallic Co reveal the confined crystal growth, due to the underlying RGO sphere structure, during the reduction process. The mean crystallite size of Co in the Co-RGO composite, calculated from the width of the (220) peak using the Scherrer equation, was 18.7 nm. Peaks of metallic Co were not observed in the XRD pattern of the powder obtained after the oxidation process at 300 °C, indicating that the metallic Co was fully transformed into the cubic Co_3O_4 phase by nanoscale Kirkendall diffusion. The mean crystallite sizes of Co_3O_4 in the Co_3O_4-RGO composite powder, obtained before and after nanoscale Kirkendall diffusion, as calculated from the width of the (311) peak using the Scherrer equation, were 7.9 nm. The full oxidation of Co into Co_3O_4 and reduction of GO into RGO during the preparation process of the Co_3O_4 nanobubble-decorated RGO spheres are further supported by the XPS spectra shown in Figures S2, 3b and c. The XPS spectrum shown in Figure 3b shows two main peaks at binding energies of 780.0 eV for Co $2p_{3/2}$ and 794.9 eV for Co $2p_{1/2}$ with two

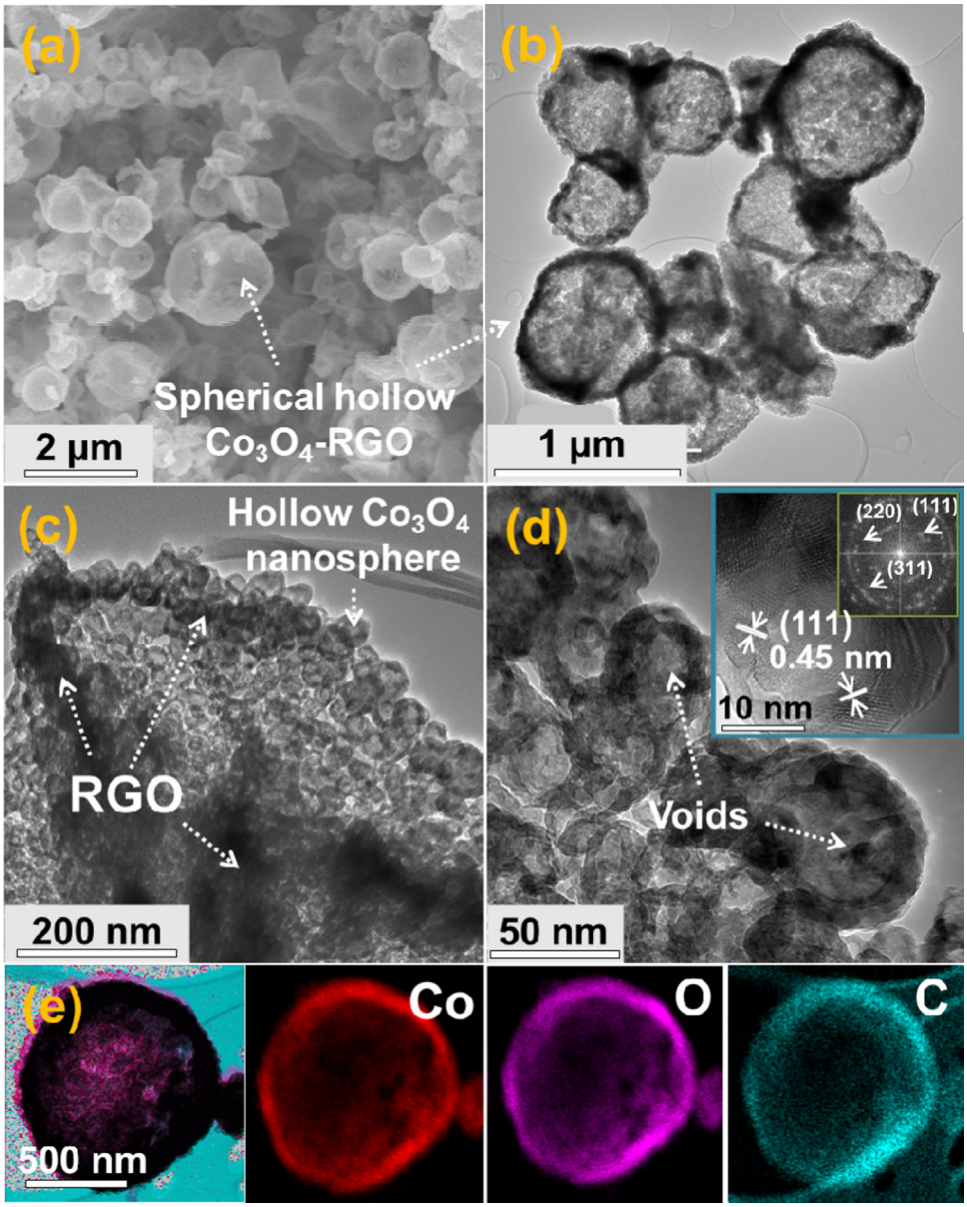

Figure 2 Morphologies, SAED, and elemental mapping images of the Co_3O_4-nanobubble-decorated RGO spheres. (a) SEM image; (b,c) TEM images; (d) HR-TEM image and SAED pattern; and (e) elemental mapping images.

shakeup satellites (denoted as "Sat."), which are the characteristic peaks of cubic-phase Co_3O_4 [50]. The C 1s peaks shown in Figure 3c can be attributed to sp^2-bonded carbon (C–C), epoxy and alkoxy groups (C–O), and carbonyl and carboxylic (C═O) groups, which corresponded to peaks at 284.6, 286.6, and 288.1 eV, respectively. The XPS spectrum shows a sharp peak at 284.6 eV, which is assigned to the C–C bonds throughout the RGO. The sharp C–C bond peak and weak C–O and C═O peaks reveal the thermal reduction of GO nanosheets to RGO nanosheets [51].

The thermogravimetric (TG) curve of the Co_3O_4-nanobubble-decorated RGO spheres is shown in Figure S3. The TG curve shows three weight losses by the evaporation of adsorbed water molecules and combustion of RGO. The combustion of RGO occurred in two steps. The RGO layers that were completely protected by hollow Co_3O_4 nanospheres combusted at high temperatures around 610 °C. The content of RGO in the Co_3O_4-nanobubble-decorated RGO spheres, estimated from the TG curve, was as low as 5.0 wt%. Therefore, the Co_3O_4-nanobubble-decorated RGO sphere contained a large amount of active material with a hollow nanosphere structure. The RGO contents in RGO materials composited with hollow metal oxide nanopowders prepared by hydrothermal and precipitation methods were as high as 34 and 35 wt%, respectively [46,47]. N_2 adsorption and desorption isotherms and Barrett–Joyner–Halenda (BJH) pore-size distributions of the cobalt oxide–RGO composite powder obtained before and after nanoscale Kirkendall diffusion are shown in Figures S4 and 3d, respectively. The Co_3O_4-nanobubble-decorated RGO spheres had mesopores with a maximum pore diameter of 12 nm. However, the CoO/Co_3O_4–RGO composite powders directly prepared by spray pyrolysis had mesopores with a maximum pore diameter of 4 nm. The BET surface areas of the Co_3O_4–RGO

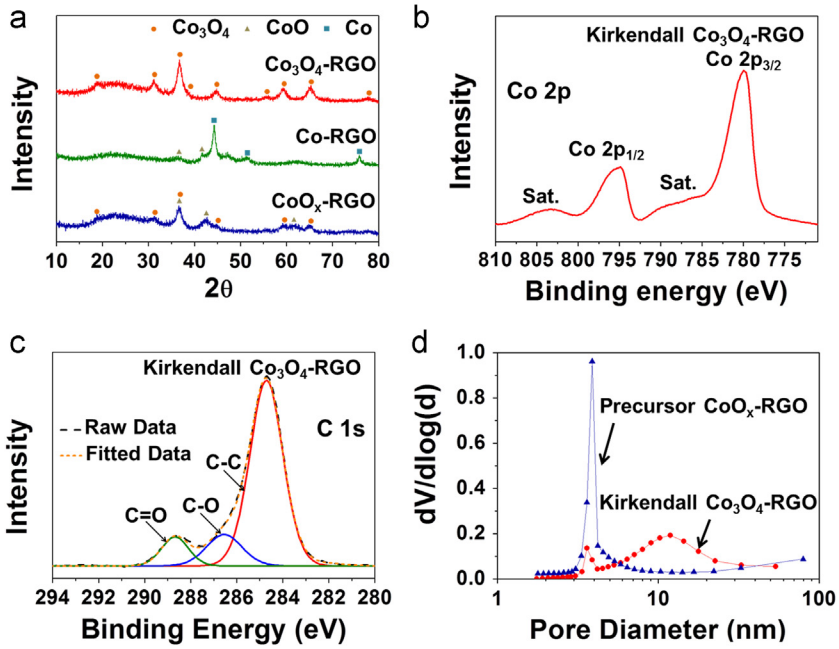

Figure 3 Properties of the cobalt oxide–RGO spheres obtained before and after nanoscale Kirkendall diffusion process. (a) XRD patterns; (b) XPS spectrum of Co 2p; (c) XPS spectrum of C 1s; and (d) pore size distributions.

composite powders obtained before and after nanoscale Kirkendall diffusion were 78 and 47 $m^2 g^{-1}$, respectively. The crystal growth of Co_3O_4 during the two-step post-treatment process decreased the BET surface area of the Co_3O_4-nanobubble-decorated RGO spheres.

Figure 4a and b shows the cyclic voltammograms (CVs) of the Co_3O_4-RGO composite powders obtained before and after nanoscale Kirkendall diffusion for the first five charge/discharge cycles at a scan rate of 0.07 mV s^{-1}. The CV profile of the CoO/Co_3O_4-RGO composite that was prepared directly by spray pyrolysis displays three reduction peaks at 0.63, 0.85, and 0.95 V in the first discharging process. The reduction peaks at 0.95 and 0.63 V were attributed to Li^+ insertion into CoO and the conversion reaction between CoO and Li^+ to form metallic Co and Li_2O, respectively [52,53]. The reduction peak observed at 0.85 V was attributed to Li^+ insertion into the crystal structure of Co_3O_4 and the conversion reaction between Co_3O_4 and Li^+ to form metallic Co and Li_2O [54]. The CV profile shown in Figure 4a also displays the mixed crystal structure of CoO and Co_3O_4 phases in the CoO/Co_3O_4-RGO composite powder prepared directly by spray pyrolysis. The CV profile of the Co_3O_4-nanobubble-decorated RGO spheres obtained after nanoscale Kirkendall diffusion shows one sharp reduction peak at 0.85 V in the first discharging process, attributed to Li^+ insertion into the crystal structure of Co_3O_4 and the conversion reaction between Co_3O_4 and Li^+ to form metallic Co and Li_2O. The broad anodic peaks at around 2.2 V in the first charge scan of both samples can be attributed to the regeneration of CoO [53]. The reduction peaks observed at 0.9 and 1.2 V for both samples from the second cycle onward were attributed to Li^+ insertion into CoO and the conversion reaction between CoO and Li^+ to form metallic Co and Li_2O, respectively [54]. The prominently overlapping CV profiles from the second cycle onward reveal the superior cycling ability of the Co_3O_4-nanobubble-decorated RGO spheres obtained through nanoscale Kirkendall diffusion. The initial discharge and charge curves of the two samples at a high current density of 2 A g^{-1} are shown in Figure 4c. The Co_3O_4-nanobubble-decorated RGO spheres exhibited a long plateau region in the initial discharge profile at a voltage of approximately 1 V, corresponding to Li^+ insertion into the crystal structure of Co_3O_4 and reduction of the Co ions to Co metal [55]. Meanwhile, two distinct regions are observed in the initial discharge profile of the CoO/Co_3O_4-RGO composite powders obtained before nanoscale Kirkendall diffusion. The first plateau at 0.9 V is associated with Li^+ insertion into CoO and Co_3O_4 and the conversion reaction between Co_3O_4 and Li^+ [55]. The second plateau located at 0.6 V is ascribed to the conversion reaction between CoO and Li^+ [56]. The cobalt oxide–RGO composite powders obtained before and after nanoscale Kirkendall diffusion showed initial discharge capacities of 1455 and 1471 mA h g^{-1}, respectively, and initial Coulombic efficiencies of 72 and 77%, respectively. The cycling performances of the two samples at a constant current density of 2 A g^{-1} are shown in Figure 4d. The cobalt oxide–RGO composite powders obtained before and after nanoscale Kirkendall diffusion showed discharge capacities at the 200th cycle of 932 and 1156 mA h g^{-1}, respectively; capacity retentions from the second cycle onward were 89 and 99%, respectively. The electrode density of the Co_3O_4-nanobubble-decorated RGO spheres was 1.02 g cm^{-3}. The volumetric discharge capacity of the Co_3O_4-nanobubble-decorated RGO spheres at the 200th cycle was 1179 mA h cm^{-3}. The rate performances of the two samples are shown in Figure 4e, in which the current density was increased step-wise from 1 to 10 A g^{-1}, with a step size of 1 A g^{-1}. The two samples had

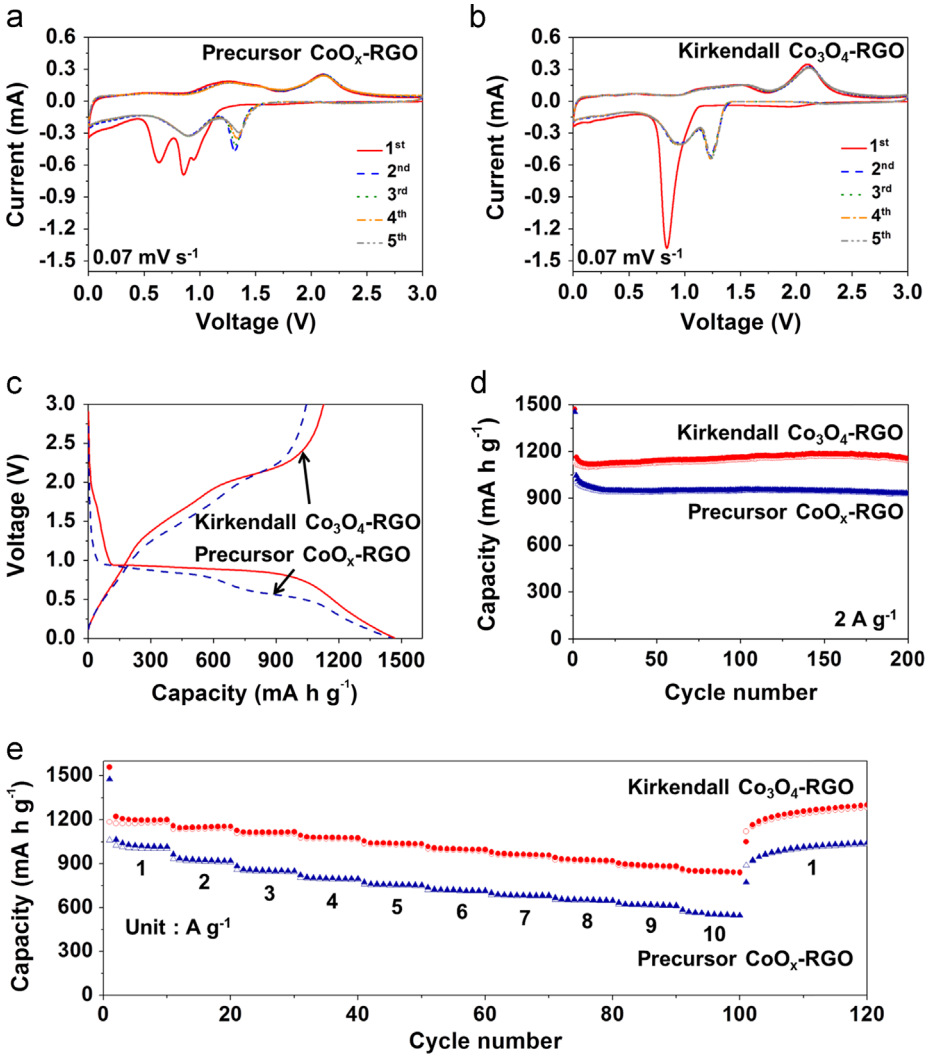

Figure 4 Electrochemical properties of the cobalt oxide-RGO spheres obtained before and after nanoscale Kirkendall diffusion process. (a) CV curves of the CoO_x-RGO; (b) CV curves of the Co_3O_4-RGO; (c) initial charge and discharge curves at a current density of 2 A g^{-1}; (d) cycling performances at a current density at 2 A g^{-1}; and (e) rate performances.

good rate performances and good capacity recovery properties when the current density returned to 1 A g^{-1}, even after cycling at high current densities. However, the capacity gaps between the two samples increased with increasing current densities. The Co_3O_4-nanobubble-decorated RGO spheres had superior rate performance compared with that of the CoO/Co_3O_4-RGO composite powder prepared directly by spray pyrolysis. The final discharge capacities of the Co_3O_4-nanobubble-decorated RGO spheres at current densities of 1, 3, 5, 7, and 10 A g^{-1} were 1200, 1117, 1036, 959, and 842 mA h g^{-1}, respectively. The discharge capacities decreased slightly with increasing current densities. The rate performances of the two samples are also shown in Figure S6, with the current density increased stepwise from 0.1 to 10 A g^{-1} and with one cycle performed at each step. The capacity gaps between the two samples clearly increased with increasing current densities.

Electrochemical impedance spectroscopy (EIS) was conducted to confirm the superior electrochemical properties of the Co_3O_4-nanobubble-decorated RGO spheres compared to the CoO/Co_3O_4-RGO composite prepared by spray pyrolysis. The impedance measurements of the two samples were carried out at room temperature before and after 100 cycles at a current density of 2 A g^{-1}. The resulting Nyquist plots shown in Figure 5a and b show semicircles in the medium-frequency range, which are assigned to the charge-transfer resistance of the electrodes, and lines inclined at $\sim 45^{\circ}$ to the real axis at low frequencies, which correspond to Li^+ diffusion within the electrode [57,58]. The Co_3O_4-nanobubble-decorated RGO spheres had a slightly higher charge transfer resistance before cycling, compared to the CoO/Co_3O_4-RGO composite prepared directly by spray pyrolysis. However, the opposite result was obtained after 100 cycles, as shown in Figure 5b. The Co_3O_4-nanobubble-decorated RGO sphere had superior structural stability compared with the CoO/Co_3O_4-RGO composite powders prepared directly by spray pyrolysis. The relationships between the real part of the impedance spectra (Z_{re}) and $\omega^{-1/2}$ (where ω is the angular frequency in the low-frequency region, given by $\omega = 2\pi f$) before and after 100 cycles are shown in Figure 5c and d respectively. The Co_3O_4-nanobubble-decorated RGO sphere had a faster Li^+ diffusion rate than the CoO/Co_3O_4-RGO composite powders

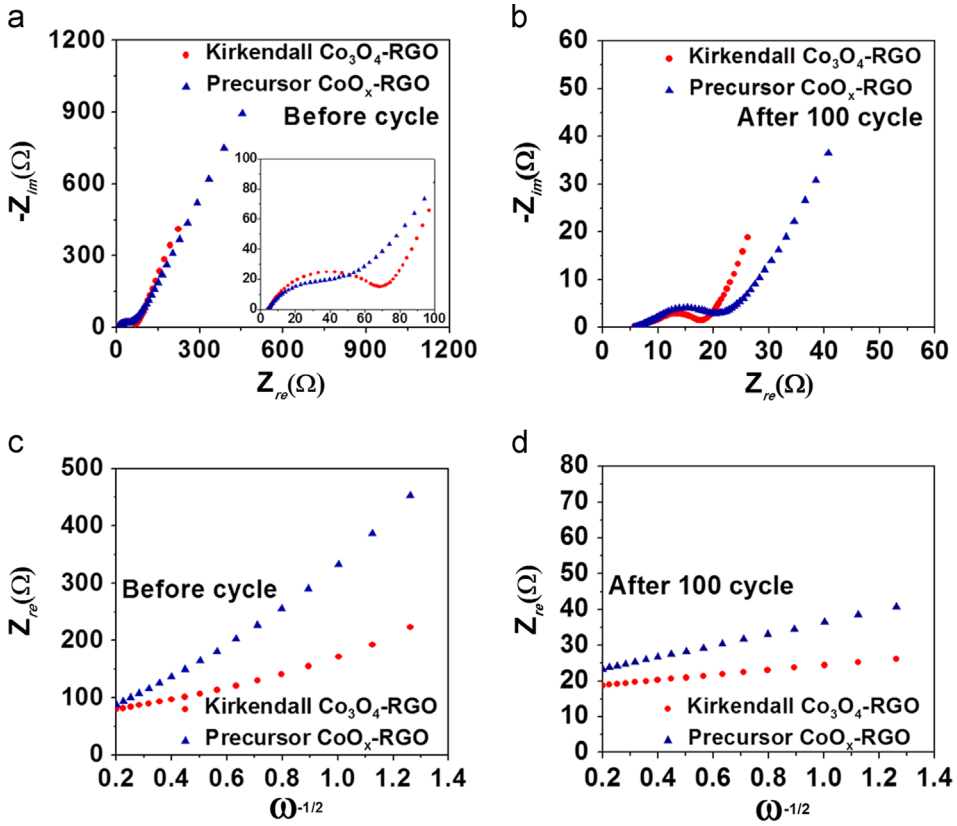

Figure 5 Electrochemical impedance spectroscopy (EIS) and relationship between Z_{re} and $\omega^{-1/2}$ in the low-frequency region. (a,b) EIS spectra before cycling and after 100th cycle; and (c,d) linear fits in the low-frequency region before cycling and after 100th cycle.

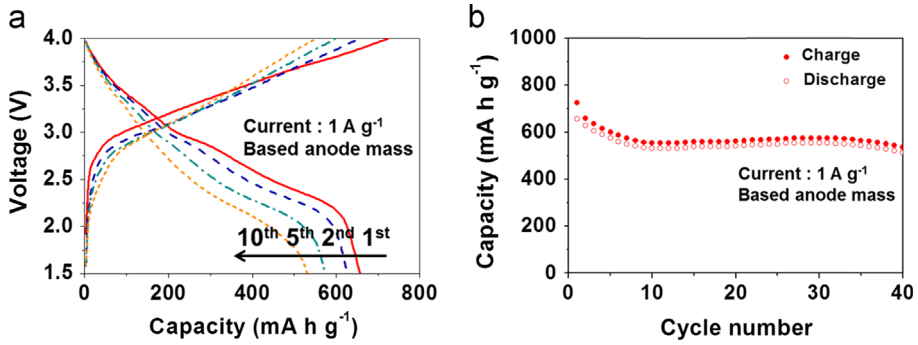

Figure 6 Electrochemical properties of a full cell of anode (the Co_3O_4-nanobubble-decorated RGO spheres)/cathode ($LiMn_2O_4$). (a) charge-discharge curves at a current density of 1 A g^{-1}; (b) cycling performance at a current density at 1 A g^{-1} based on the anode (Co_3O_4-nanobubble-decorated RGO spheres) mass.

prepared directly by spray pyrolysis, before and after cycling. The morphologies of the Co_3O_4-nanobubble-decorated RGO spheres obtained after 100 cycles at a current density of 2 A g^{-1} are shown in Figure S7. The overall morphology of the Co_3O_4-nanobubble-decorated RGO spheres was maintained even after cycling as shown by FE-SEM images. The hollow structure of Co_3O_4 nanobubble decorating the RGO was also maintained even after cycling as shown by TEM image. Therefore, the Co_3O_4-nanobubble-decorated RGO spheres, with high structural stability and good Li^+ diffusion rate, showed good cycling and rate performances.

To show the composite's ability for practical application, the Co_3O_4-nanobubble-decorated RGO spheres anode was prelithiated and combined with a high voltage $LiMn_2O_4$ cathode to construct a full Li-ion cell. In this study, $LiMn_2O_4$ yolk-shell powders with a distinctive core@void@shell configuration prepared by spray pyrolysis process were used [59]. The morphologies and crystal structures of the yolk-shell $LiMn_2O_4$ powders prepared by spray pyrolysis before and after post-treatment at 650 °C are shown in Figure S8. The electrochemical properties of the $LiMn_2O_4$ yolk-shell powders post-treated at 650 °C are shown in Figure S9. The charge/discharge curves and cycling performance of Co_3O_4-nanobubble-decorated RGO spheres/$LiMn_2O_4$ yolk-shell full cells with a cut-off voltage range of 1.5–4.0 V are shown in Figure 6. As shown in Figure 6a, these materials can exhibit

charge and discharge capacities of about 726 and 657 mA h g^{-1}, respectively, at the first cycle at a current density of 1 A g^{-1}, based on the mass of Co_3O_4-nanobubble-decorated RGO spheres anode. The Coulombic efficiency of the cell in the initial cycle was 90%, and it increased quickly to close to an average value of 96% in the following cycles. The reason for the low initial Coulombic efficiency and capacity fading during the first 10 cycles may be because of the decomposition of electrolyte and the formation of a solid electrolyte interface (SEI) layer at the high charge voltage. After capacity fading during the first 10 cycles, the cell demonstrated a good cycling performance with capacity retention of 96.7%. However, the electrochemical properties of the cathode powders should be optimized to achieve the long cycling performance of the Co_3O_4-nanobubble-decorated RGO spheres/$LiMn_2O_4$ yolk–shell full cells.

Conclusions

In summary, Co_3O_4-nanobubble-decorated RGO spheres were prepared by a three-step process. The CoO_x–RGO spheres prepared directly by spray pyrolysis were transformed into Co_3O_4-nanobubble-decorated RGO spheres by a two-step post-treatment heating process. CoO/Co_3O_4 nanocrystals were transformed into Co_3O_4 hollow nanospheres through the oxidation of Co metal nanopowder by the well-known nanoscale Kirkendall diffusion process. The hollow structure of the RGO spheres was maintained during the two-step post-treatment process. The size of the Co_3O_4 hollow nanospheres and the RGO content in the Co_3O_4-nanobubble-decorated RGO spheres could be easily controlled by changing the preparation conditions, such as the GO content in the spray solution, temperature of the spray pyrolysis process, and reduction temperatures. The simple process introduced in this study could be used to prepare metal oxide nanobubble-decorated RGO spheres with various compositions for many applications, including energy storage.

Acknowledgments

This work was supported by the Energy Efficiency & Resources Core Technology Program of the Korea Institute of Energy Technology Evaluation and Planning (KETEP), Granted financial resource from the Ministry of Trade, Industry & Energy, Republic of Korea (201320200000420).

Appendix A. Supporting information

Supplementary data associated with this article can be found in the online version at http://dx.doi.org/10.1016/j.nanoen.2015.07.026.

References

[1] N. Liu, Z. Lu, J. Zhao, M.T. McDowell, H.W. Lee, W. Zhao, Y. Cui, Nat. Nanotechnol. 9 (2014) 187–192.
[2] M.T. McDowell, S.W. Lee, W.D. Nix, Y. Cui, Adv. Mater. 25 (2013) 4966–4985.
[3] M.V. Reddy, G.V.S. Rao, B.V.R. Chowdari, Chem. Rev. 113 (2013) 5364–5457.
[4] H.S. Kim, G.J. Jeong, Y.U. Kim, J.H. Kim, C.M. Park, H.J. Sohn, Chem. Soc. Rev. 42 (2013) 9011–9034.
[5] J. Jiang, Y.Y. Li, J.P. Liu, X.T. Huang, C.Z. Yuan, X.W. Lou, Adv. Mater. 24 (2012) 5166–5180.
[6] L. Zhang, H.B. Wu, X.W. Lou, Adv. Energy Mater. 4 (2014) 1300958.
[7] Y. Li, B. Tan, Y. Wu, Nano Lett. 8 (2008) 265–270.
[8] H. Wang, L.F. Cui, Y. Yang, H.S. Casalongue, J.T. Robinson, Y. Liang, Y. Cui, H. Dai, J. Am. Chem. Soc. 132 (2010) 13978–13980.
[9] X. Wang, X.L. Wu, Y.G. Guo, Y. Zhong, X. Cao, Y. Ma, J. Yao, Adv. Funct. Mater. 20 (2010) 1680–1686.
[10] J. Wang, N. Yang, H. Tang, Z. Dong, Q. Jin, M. Yang, D. Kisailus, H. Zhao, Z. Tang, D. Wang, Angew. Chem. Int. Ed. 52 (2013) 6417–6420.
[11] G. Gao, H.B. Wu, X.W. Lou, Adv. Energy Mater. 4 (2014) 1400422.
[12] P. Roy, S.K. Srivastava, J. Mater. Chem. A 3 (2015) 2454–2484.
[13] K. Zhang, X. Han, Z. Hu, X. Zhang, Z. Tao, J. Chen, Chem. Soc. Rev. 44 (2015) 699–728.
[14] Y.J. Hong, M.Y. Son, Y.C. Kang, Adv. Mater. 25 (2013) 2279–2283.
[15] S. Xin, Y.G. Guo, L.J. Wan, Acc. Chem. Res. 45 (2012) 1759–1769.
[16] W.M. Zhang, J.S. Hu, Y.G. Guo, S.F. Zheng, L.S. Zhong, W.G. Song, L.J. Wan, Adv. Mater. 20 (2008) 1160–1165.
[17] Z. Wang, D. Luan, F.Y.C. Boey, X.W. Lou, J. Am. Chem. Soc. 133 (2011) 4738–4741.
[18] J.C. Park, J.H. Kim, H.S. Kwon, H.J. Song, Adv. Mater. 21 (2009) 803–807.
[19] B. Koo, H. Xiong, M.D. Slater, V.B. Prakapenka, M. Balasubramanian, P. Podsiadlo, C.S. Johnson, T. Rajh, E.V. Shevchenko, Nano Lett. 12 (2012) 2429–2435.
[20] J. Liu, Y. Li, H. Fan, Z. Zhu, J. Jiang, R. Ding, Y. Hu, X. Huang, Chem. Mater. 22 (2010) 212–217.
[21] X. Zhou, Y.X. Yin, L.J. Wan, Y.G. Guo, J. Mater. Chem. 22 (2012) 17456–17459.
[22] L. Zhang, H.B. Wu, X.W. Lou, J. Am. Chem. Soc. 135 (2013) 10664–10672.
[23] R. Wu, X. Qian, K. Zhou, J. Wei, J. Lou, P.M. Ajayan, ACS Nano 8 (2014) 6297–6303.
[24] W.S. Kim, Y. Hwa, H.C. Kim, J.H. Choi, H.J. Sohn, S.H. Hong, Nano Res. 7 (2014) 1128–1136.
[25] M. Sasidharan, N. Gunawardhana, C. Senthil, M. Yoshio, J. Mater. Chem. A 2 (2014) 7337–7344.
[26] J. Hu, M. Chen, X. Fang, L. Wu, Chem. Soc. Rev. 40 (2011) 5472–5491.
[27] X.M. Sun, J.F. Liu, Y.D. Li, Chem. Eur. J. 12 (2006) 2039–2047.
[28] J.G. Railsback, A.C.J. Peck, J.W. Wang, J.B. Tracy, ACS Nano 4 (2010) 1913–1920.
[29] L. Hu, N. Yan, Q.W. Chen, P. Zhang, H. Zhong, X.R. Zheng, Y. Li, X. Hu, Chem. Eur. J. 18 (2012) 8971–8977.
[30] R.K. Chiang, R.T. Chiang, Inorg. Chem. 46 (2007) 369–371.
[31] Y.M. Lee, M.R. Jo, K.S. Song, K.M. Nam, J.T. Park, Y.M. Kang, ACS Appl. Mater. Interfaces 4 (2012) 3459–3464.
[32] Y.D. Yin, R.M. Rioux, C.K. Erdonmez, S. Hughes, G.A. Somorjai, A.P. Alivisatos, Science 304 (2004) 711–714.
[33] H.J. Fan, M. Knez, R. Scholz, D. Hesse, K. Nielsch, M. Zacha Gosele, Nano Lett. 7 (2007) 993–997.
[34] H.J. Fan, U. Gosele, M. Zacharias, Small 3 (2007) 1660–1671.
[35] B.D. Anderson, J.B. Tracy, Nanoscale 6 (2014) 12195–12216.
[36] Y.W. Zhu, S.T. Murali, W.W. Cai, X.S. Li, J.W. Suk, J.R. Potts, R.S. Ruoff, Adv. Mater. 22 (2010) 3906–3924.
[37] K.Y. Shin, J.S. Jang, Chem. Commun. 50 (2014) 6645–6648.
[38] S. Han, D.Q. Wu, S. Li, F. Zhang, X.L. Feng, Adv. Mater. 26 (2014) 849–864.
[39] G. Fugallo, A. Cepellotti, L. Paulatto, M. Lazzeri, N. Marzari, F. Mauri, Nano Lett. 14 (2014) 6109–6114.

[40] L.F. Cui, J. Shen, F.Y. Cheng, Z.L. Tao, J. Chen, J. Power Sources 196 (2011) 2195–2201.
[41] Z.Q. Zhu, S.W. Wang, J. Du, Q. Jin, T. Zhang, F.Y. Cheng, J. Chen, Nano Lett. 14 (2014) 153–157.
[42] J. Qin, C.N. He, N.Q. Zhao, Z.Y. Wang, C.S. Shi, E.Z. Liu, J.J. Li, ACS Nano 8 (2014) 1728–1738.
[43] S.H. Choi, Y.C. Kang, Carbon 79 (2014) 58–66.
[44] S.H. Choi, Y.C. Kang, ChemSusChem 7 (2014) 523–528.
[45] S.H. Choi, Y.C. Kang, Chem. Eur. J. 20 (2014) 6294–6301.
[46] S.B. Yang, G.L. Cui, S.P. Pang, Q. Cao, U. Kolb, X.L. Feng, J.C. Maier, K. Mullen, ChemSusChem 3 (2010) 236–239.
[47] J.S. Zhou, L.L. Ma, H.H. Song, B. Wu, X.H. Chen, Electrochem. Commun. 13 (2011) 1357–1360.
[48] Z.Y. Sun, K.P. Xie, Z.A. Li, I. Sinev, P. Ebbinghaus, A. Erbe, M. Farle, W. Schuhmann, M. Muhler, E. Ventosa, Chem. Eur. J. 20 (2014) 2022–2030.
[49] X.Y. Zhou, J.J. Shi, Y. Liu, Q.M. Su, J. Zhang, G.H. Du, J. Alloy. Compd. 615 (2014) 390–394.
[50] Y.J. Tak, K.J. Yong, J. Phys. Chem. C 112 (2008) 74–79.
[51] M. Beidaghi, C. Wang, Adv. Funct. Mater. 22 (2012) 4501–4510.
[52] X. Guan, J.W. Nai, Y.P. Zhang, P.X. Wang, J. Yang, L.R. Zheng, J. Zhang, L. Guo, Chem. Mater. 26 (2014) 5958–5964.
[53] F. Li, Q.Q. Zou, Y.Y. Xia, J. Power Sources 177 (2008) 546–552.
[54] G.D. Park, J.H. Lee, J.K. Lee, Y.C. Kang, Nano Res. 7 (2014) 1738–1748.
[55] X.W. Lou, D. Deng, J.Y. Lee, L.A. Archer, J. Mater. Chem. 18 (2008) 4397–4401.
[56] X.L. Huang, R.Z. Wang, D. Xu, Z.L. Wang, H.G. Wang, J.J. Xu, Z. Wu, Q.C. Liu, Y. Zhang, X.B. Zhang, Adv. Funct. Mater. 23 (2013) 4345–4353.
[57] Y.N. Ko, S.B. Park, K.Y. Jung, Y.C. Kang, Nano Lett. 13 (2013) 5462–5466.
[58] X.Y. Du, W. He, X.D. Zhang, Y.Z. Yue, H. Liu, X.G. Zhang, D.D. Min, X.X. Ge, Y. Du, J. Mater. Chem. 22 (2012) 5960–5969.
[59] C.M. Sim, S.H. Choi, Y.C. Kang, Chem. Commun. 49 (2013) 5978–5980.

Gi Dae Park received his B.S. degree from the Department of Chemical Engineering, Konkuk University, Korea in 2014. He is currently a Ph.D. candidate in the Department of Materials Science and Engineering, Korea University, Korea. His research focuses on the development of nanostructured electrode materials for lithium and sodium ion batteries using spray pyrolysis and spray drying processes.

Jung Sang Cho is a postdoctoral research fellow at the Nano Electronic Materials Laboratory, Department of Materials Science and Engineering, Korea University, Korea under Prof. Yun Chan Kang's supervision. He received his Ph.D. from the Interdisciplinary Program for Bioengineering, College of Engineering, Seoul National University, Korea in 2013. His research interests focuses on the design, synthesis, and characterization of the nanostructured materials for the energy storage, sensor, and display by using spray pyrolysis, spray drying, and electrospinning processes.

Yun chan Kang received his Ph.D. from Chemical Engineering, Korea Advanced Institute of Science and Technology (KAIST), Korea in 1997, and had post-doc experience at the Chemical Engineering, Hiroshima University in Japan (1997-1998). He returned to Korea, and joined KRICT as a senior researcher (2000-2003). He became a Professor of the Department of Chemical Engineering, Konkuk University, Korea (2004-2014). He is currently a Professor of the Department of Materials Science and Engineering, Korea University, Korea since 2014. His research group works on the development of nanostructured materials for the energy storage, sensor, catalyst, and display. For details please see the lab website: http://spray.korea.ac.kr.